Latest Miocene transtensional rifting of northeast Isla Tiburón, eastern margin of the Gulf of California

Scott E.K. Bennett[1,*], *Michael E. Oskin*[1], *Alexander Iriondo*[2,3]

1–Department of Earth and Planetary Sciences, University of California–Davis, 2119 Earth and Physical Sciences, One Shields Avenue, Davis, California 95616, USA

2–Centro de Geociencias, Universidad Nacional Autónoma de México, Campus Juriquilla, C.P. 76230 Juriquilla, Querétaro, México

3–The University of Texas at Austin, Jackson School of Geosciences, 2305 Speedway, Stop C1160, Austin, Texas 78712, USA

* Now at U.S. Geological Survey, Department of Earth and Space Sciences, University of Washington, Box 351310, Seattle, Washington 98195, USA.

ABSTRACT

The timing and kinematics of rifting are crucial to understand the conditions that led to continental rupture and formation of the Gulf of California ocean basin. We integrate detailed geologic and structural mapping, basin analysis, and geochronology, to characterize transtensional rifting on northeastern Isla Tiburón, a proximal onshore exposure of the rifted North America margin, adjacent to the axis of the Gulf of California. Slip on the Kunkaak normal fault tilted its hanging wall down-to-the-east ~70° and formed the non-marine Tecomate basin in its hanging wall, deposited across a ~20° angular unconformity. From 7.1–6.4 Ma, the hanging wall tilted at ~36°/Myr, while non-marine sandstone and conglomerate accumulated at ~1.4 mm/yr. At least 1.8 ± 0.1 km of sediments and pyroclastic deposits accumulated in the Tecomate basin concurrent with ~2.8 km of total dip-slip motion on the Kunkaak fault. Linear extrapolation of these rates suggests that fault activity and basin deposition may have initiated ca. 7.6 ± 0.2 Ma, but an older history involving initially slower rates is permissible. Paleomagnetic data indicate that ~70% of the 29° of post-12 Ma, clockwise vertical-axis rotation occurred prior to 6.4 Ma. The Kunkaak fault and Tecomate basin are truncated by the NW-striking, dextral-oblique Yawassag fault, which accrued >8 km of post-6.4 Ma dextral displacement. Structures on northeastern Isla Tiburón are the continuation of the Sacrificio fault and Coastal Sonora fault zone mapped to the southeast on mainland Sonora, which accrued several tens of kilometers of dextral offset in latest Miocene time. The establishment of rapid, latest Miocene transtension in the Coastal Sonora fault zone was synchronous with the 8–7 Ma onset of transform faulting and basin formation along the nascent Pacific-North America plate boundary throughout northwest Mexico and

40 southern California and ultimately led to continental rupture in the Gulf of California ca.
41 6 Ma.
42
43 **Keywords:** Gulf of California; oblique continental rifting; transtension; Isla Tiburón;
44 Tecomate basin; Coastal Sonora fault zone; Gulf of California shear zone
45
46 **1. INTRODUCTION**

47 The Gulf of California rift is an active oblique rift between the Pacific (PAC) and
48 North America (NAM) plates (Lonsdale, 1989) that initiated in Miocene time (ca. 12.3
49 Ma; Stock and Molnar, 1988; Atwater and Stock, 1998). As the Rivera triple junction
50 migrated towards the southeast (Nicholson et al., 1994), the NAM plate margin evolved
51 from subduction and back-arc extension to a broad region of integrated transtensional
52 dextral shearing (Seiler et al., 2010) that has been kinematically linked to the southern
53 San Andreas fault system in southern California (Larsen et al., 1968). Transtensional
54 faulting related to Miocene to present PAC-NAM relative motion, in the form of
55 clockwise vertical-axis block rotations and significant dextral strike-slip faults, has been
56 documented both east and west of the stable Baja California microplate (Spencer and
57 Normark, 1979; Gans, 1997; Oskin and Stock, 2003a; Seiler et al., 2010; Dorsey et al.,
58 2011; Bennett et al., 2013; Bennett et al., 2016). However, the spatial and temporal
59 development of focused dextral shear east of the Baja California microplate remains
60 incompletely documented, and it is unclear whether these structures played a significant
61 role in the subsequent formation of the Gulf of California ocean basin (Umhoefer, 2011).

This paper documents the timing and kinematics of transtensional fault activity on northeastern Isla Tiburón, a proximal onshore exposure of the rifted North America margin, adjacent to the axis of the Gulf of California. Here, our synthesis of new geologic and structural mapping, basin analysis, and geochronology indicates that dextral shear, evidenced by clockwise block rotation and strike-slip faulting, initiated during latest Miocene time and was related to the transtensional Coastal Sonora fault zone. These observations contribute to a growing collection of evidence that the PAC-NAM plate boundary progressively coalesced into the Gulf of California shear zone during latest Miocene time (see Bennett et al., 2016 for summary). This narrow transtensional belt subsequently hosted the incursion of the Gulf of California marine seaway (Oskin and Stock, 2003b) and was the site of localized oblique rifting between the Baja California microplate and mainland México. Rifted fragments of the Gulf of California shear zone, now preserved on the margins of the Gulf of California, record a consistent history of the plate boundary conditions that presaged successful continental rupture during latest Miocene time (Lizarralde et al., 2007; Martín-Barajas et al., 2013).

2. TECTONIC SETTING

Isla Tiburón is an uninhabited island in the north-central Gulf of California and is the westernmost terrestrial exposure of the rifted edge of North America continental crust within the Upper Delfín-Upper Tiburón rift segment (Fig. 1). Two, significant, rift-related strike-slip fault zones occur near the Sonoran shoreline and continue across Isla Tiburón: the La Cruz fault on southern part of the island (Gastil and Krummenacher, 1977a, b; Oskin, 2002; Bennett et al., 2016), and the Yawassag fault on the northeastern

part of the island (Gastil and Krummenacher, 1977a, b; this study). These strike-slip fault zones continue towards the southeast for several tens of kilometers (Aragón-Arreola et al., 2005; Bennett et al., 2013), suggesting they were significant, plate boundary-scale structures prior to rift localization. These NW-striking dextral-oblique structures also continue towards the northwest, offshore of Isla Tiburón, and are kinematically linked to the De Mar fault and the Tiburón transform, respectively (Mar-Hernandez et al., 2012). Thus, the onshore exposures of these faults on Isla Tiburón represent the principal transform boundaries of the Upper Delfín–Upper Tiburón rift segment (Figs. 1 and 2; Gastil and Krummenacher, 1977a; Lonsdale, 1989; Fenby and Gastil, 1991).

3. METHODS

3.1. Geologic, Structural, and Stratigraphic Mapping

Building upon reconnaissance mapping by Gastil and Krummenacher (1977a) and Oskin (2002) (Fig. 2), we present geologic mapping (Fig. 3) and tectono-stratigraphic analysis of northeastern Isla Tiburón. The NW-striking Yawassag fault divides northeastern Isla Tiburón into two structural domains: the Hinzime domain to the northeast, and the Sierra Kunkaak domain to the southwest (Fig. 4). Structural measurements include brittle-fault orientations and kinematic indicators such as fault striae preserved on polished fault planes (Fig. 3). Mapping was conducted at 1:10,000-scale on 0.6 m-resolution, pan-sharpened Quickbird satellite imagery with topographic contours derived from the 90-m Shuttle Radar Topography Mission digital elevation model, similar to Bennett et al. (2015) and Bennett et al., (2016).

3.2. Geochronology

We conducted U/Pb (zircon) and Ar/Ar (k-feldspar) analysis on a sample of the Tecomate ash bed (identified and named in this study) intercalated within the Tecomate basin (Figs. 5 and 6; Table 1 and 2), which was processed as described by Bennett et al. (2015). Additional age constraints on northeastern Isla Tiburón come from published geochronologic ages from plutonic rocks and our correlation of two regional ignimbrites that underlie and are interbedded within Tecomate basin deposits and are well-dated elsewhere in the Gulf of California. Collectively, these geochronologic ages provide timing constraints for faulting and related basin formation on northeastern Isla Tiburón.

4. STRATIGRAPHY

4.1. Pre-Cenozoic Rocks

Pre-Cenozoic rocks on northeastern Isla Tiburón consist of pre-Cambrian to Mesozoic(?) basement rocks (Gastil and Krummenacher, 1977b) and Cretaceous plutonic rocks and are observed on both sides of the Yawassag fault (Fig. 4). Metamorphic basement rocks consist of meta-carbonate (*Pz-carb*) and other meta-sedimentary units (*Pzms*), including slate, quartzite, and phyllite. Plutonic basement rocks on northeastern Isla Tiburón consist predominantly of tonalite (*Kt*) and related, typically felsic, dikes. Subordinate exposures of granodiorite and diorite composition are observed in the southernmost portion of the study area, southwest of the Yawassag fault (Fig. 3). Niño-Estrada et al. (2014) report U-Pb (zircon) ages of 83.4 ± 0.9 Ma and 84.4 ± 0.9 Ma from tonalite (*Kt*) exposures in the Hinzime domain (Fig. 3). Gastil and Krummenacher (1977b) report a K-Ar (hornblende) age of 90.4 ± 2.7 Ma from a tonalite exposure in the Sierra Kunkaak domain. Nearby, Schaaf et al. (1999) report two Rb-Sr (biotite-whole

rock) cooling ages of 81.4 ± 3.2 Ma on tonalite (*Kt*) and 77.7 ± 3.1 Ma on a granodiorite that we map as diorite (*Kd*). These isotopic results from northeastern Isla Tiburón are similar to a K-Ar (hornblende) age of 84.5 ± 7.9 Ma from tonalite on northwestern Isla Tiburón (Gastil and Krummenacher, 1977b) and a U-Pb (zircon) age of 82.6 ± 0.9 Ma from tonalite on nearby Isla Patos (Fig. 2; Niño-Estrada et al., 2014).

4.2. Middle Miocene Volcanic and Sedimentary Rocks

A sequence of volcanic and sedimentary rocks of middle Miocene age nonconformably overlies basement rocks on northeastern Isla Tiburón. Previous studies correlate Miocene volcanic and sedimentary units in the Sierra Kunkaak domain, southwest of the Yawassag fault, to units in the Hinzime domain, northeast of the fault (Gastil and Krummenacher, 1977a; Oskin, 2002). Here, we summarize this volcanic and sedimentary sequence in both domains and demonstrate that these units only broadly correlate across the Kunkaak dextral-normal fault within the Sierra Kunkaak domain, and do not correlate across the Yawassag dextral fault.

4.2.1. Sierra Kunkaak Domain

In the Sierra Kunkaak domain, southwest of the Yawassag fault, middle Miocene volcanic and sedimentary rocks largely differ across the Kunkaak fault (Fig. 3). West of the Kunkaak fault, the lowest observed unit from this sequence is a basal non-marine conglomerate and sandstone unit (*Tcb*), observed discontinuously in angular and buttress unconformably contact with basement rocks (Figs. 3 and 7C). This unit likely correlates to unit '*Tcg'* in the Sierra Menor of northwestern Isla Tiburón (Oskin, 2002) and unit '*Tcb'* in coastal Sonora immediately east of Isla Tiburón (Bennett, 2009), both observed at a similar stratigraphic position. A basaltic andesite flow (*Tba*) conformably(?) overlies

Tcb. Along strike to the southeast, an andesite flow (*Tha*) is observed at the same stratigraphic position as *Tcb* and *Tba,* in nonconformable contact with basement rocks. We tentatively assign a middle Miocene age to *Tcb*, *Tba*, and *Tha*. However, these units are not isotopically dated and could possibly be early Miocene or older. Discontinuous deposits of the ~12.5 Ma Tuff of San Felipe (*Ttsf*; Stock et al., 1999) overlie these units and are locally in nonconformable contact with basement rocks as well (Fig. 3). Outcrop quality is insufficient to determine whether these contact relationships are the result of an angular unconformity between *Ttsf* and underlying units or due to paleotopography of basement rocks and discontinuous emplacement of *Tba* and *Tha*. The uppermost unit of this sequence is a discontinuous vesicular basalt flow (*Tbv*).

East of the Kunkaak fault, the lowest observed units from this sequence are a basalt flow (*Tb1*) and the lower flow of the Rhyolite Flows of Sepoc Hancaap (*Trsh1*), a purplish-red aphanitic rhyolite with 1–2 cm-spaced foliation (Figs. 3 and 7C). We tentatively assign a middle Miocene age to *Tb1* and *Trsh1*, but these units are undated and could possibly be early Miocene or older. These units are overlain by the ~12.5 Ma Tuff of San Felipe (*Ttsf*), non-marine conglomerate and sandstone (*Tcg1*), the upper flow of the Rhyolite Flows of Sepoc Hancaap (*Trsh2*), another basalt flow (*Tb2*), and ash- and pumice-rich, greenish-yellow volcaniclastic sandstone (*Tsg*).

4.2.2. Hinzime Domain

In the Hinzime domain, we map two undated volcanic units that are sparsely exposed northeast of the Yawassag fault (Figs. 3 and 7A). Gastil and Krummenacher (1977a) and Oskin (2002) mapped the Hinzime domain in reconnaissance and correlated these volcanic units with volcanic and sedimentary deposits of the Tecomate basin,

177 introduced below. In contrast, we map these volcanic units as the Rhyolite of Hast
178 Hinzime (*Trhh*) and an overlying silicified rhyolite tuff and breccia (*Tbhh*), which may be
179 the top of *Trhh*, and tentatively assign these units a Miocene age.

180 **4.3. Late Miocene–Pliocene(?) Tecomate Basin**

181 In the Sierra Kunkaak domain, a thick sequence of late Miocene to Pliocene(?)
182 volcanic and sedimentary units are exposed within an uplifted and eroded portion of the
183 Tecomate basin. Tecomate basin deposits overlie the early to middle Miocene sequence
184 above an angular unconformity with up to ~20° difference in dip. These Tecomate basin
185 deposits accumulated in a structurally related half-graben in the hanging walls of the
186 Kunkaak fault and Tecomate fault (Figs. 3, 7B, and 7C).

187 The lowest portion of the Tecomate basin is exposed just east of the Tecomate
188 fault where deposits of non-marine coarse conglomerate and sandstone (*Tcg3*) overlie
189 volcanic units of the middle Miocene sequence that are more steeply inclined (Fig. 3).
190 Deposits within the Tecomate basin display a fanning-dip geometry, where the structural
191 tilt of basin fill shallows up-section from >50° near its base to 15–20° near its top (Figs.
192 3, 7B, and 7C). The uppermost *Tcg3* deposits of the Tecomate basin are observed
193 immediately west of the Kunkaak fault, in fault contact with basement rocks and older
194 volcanic units in the footwall. From our structural cross sections B-B' and C-C' (Figs. 7B
195 and 7C), we estimate a minimum of 1.8 ± 0.1 km of non-marine conglomerate (*Tcg3*) and
196 pyroclastic material (*Tmr3, T3t, Tmr4*) accumulated within the Tecomate basin, above the
197 hanging wall of the Kunkaak normal fault. Additional, younger basin deposits may have
198 once existed, but, if present, have since been eroded from the upper part of the basin.

Three distinct volcanic units are interbedded amongst *Tcg3* sedimentary deposits of the Tecomate basin. The Tecomate ash bed is a 2 m-thick, white, reworked ash deposit interbedded within *Tcg3*, ~60–70 m stratigraphically above the basal angular unconformity (Figs. 3 and 7C). We report a new $^{40}Ar/^{39}Ar$ (K-feldspar, multiple crystals) age of 7.11 ± 0.09 Ma (Fig. 5A; Table 1), a new $^{40}Ar/^{39}Ar$ (plagioclase, multiple crystals) age of 7.00 ± 0.50 Ma (Fig. 5B; Table 1), and a U/Pb (zircon, multiple crystals) age of 7.03 ± 0.19 Ma (Fig. 6; Table 2) for the Tecomate ash bed. We prefer the $^{40}Ar/^{39}Ar$ age of 7.11 ± 0.09 Ma, because the Ar/Ar technique provides a better estimate of a true eruption age than the U/Pb technique (Simon et al., 2008). Further up-section a thick sequence of pyroclastic deposits is observed interbedded amongst *Tcg3* deposits (Figs. 3, 7B, and 7C). The base of this sequence is a 110–120 m-thick, crystal- and lithic-rich, orange, moderately- to densely-welded ash-flow tuff (*Tmr3*). Above this is 100–240 m of primary and reworked air-fall and volcaniclastic debris-flow deposits (*T3t*), capped by 25–40 m of a crystal- and lithic-poor, maroon, densely-welded ash-flow tuff (*Tmr4*). Following earlier reconnaissance mapping by Oskin (2002) and Oskin and Stock (2003a), we correlate this *Tmr3-T3t-Tmr4* volcanic sequence with the ~6.4 Ma Tuffs of Mesa Cuadrada, a regionally extensive tuff sequence that blanketed >2,100 km^2 of present-day northeastern Baja California (Stock, 1989; Lewis, 1996; Nagy et al., 1999), western and northern Isla Tiburón (Oskin et al., 2001; Oskin, 2002; Oskin and Stock, 2003a; this study), and coastal Sonora (Oskin and Martín-Barajas, 2003; Bennett et al., 2013). An additional, 2 m-thick interval of white, cross-bedded, crystal-poor, reworked ash beds occur amongst *Tcg3* conglomerate beds ~30 m stratigraphically above *Tmr4* (Fig. 3). Neither conglomerate nor pyroclastic rocks of the Tecomate basin-fill are observed east

of the Kunkaak fault. However, these deposits may exist in the subsurface east of the northern Sierra Menor, obscured beneath Quaternary deposits of the Valle de las Aguilas (Fig. 3).

4.4. Quaternary Deposits

Several young, likely Quaternary age deposits are observed across northeastern Isla Tiburón (Fig. 3). The oldest Quaternary deposits consist of non-marine alluvium (*Qoa*) and fossiliferous marine deposits (*Qm*). Thin deposits of *Qm* are observed in the lowest 2–3 m of the 10–25 m-high sea cliff along Playa Tecomate. The upper portion of this sea cliff consists of stratified non-marine alluvial deposits (*Qoa*), which include capping cross-stratified dune deposits. Inland, deposits of *Qoa* fill valley bottoms and are widespread across alluvial plains with inactive upper terrace tread surfaces. Younger fluvial sand and cobble deposits (*Qal*) are commonly found within active channels. A discontinuous strip of unconsolidated beach sand and cobble deposits (*Qb*) is found along the modern shoreline, and a veneer of unconsolidated, aeolian sand deposits (*Qae*) are found up to 5.5 km inland from Canoa Canipai (Playa Tecomate).

5. FAULTING AND FOLDING

Several Late Cenozoic structures deform rocks on northeastern Isla Tiburón. Tecomate basin deposits (e.g. *Tcg3*) accumulated in a structurally related half-graben in the hanging wall of the Kunkaak fault and Tecomate fault (Figs. 7B and 7C). These basin deposits overlie older strata across an angular unconformity and are cut by structures related to strike-slip faulting.

5.1. Kunkaak fault

The Kunkaak fault is a significant, north-northwest striking, gently- to moderately-dipping dextral-normal fault (Fig. 3). This fault juxtaposes latest Miocene volcanic and sedimentary units (e.g. *Tcg3*, *Tmr3*, *Tmr4*) in the hanging wall against mostly metasedimentary basement (e.g. *Pzms*) in the footwall. The fanning-dip geometry observed in the Tecomate basin fill suggests basin accumulation was coeval with dip-slip on the Kunkaak fault and tilting of its hanging wall. This geometry also suggests that the dip of the Kunkaak fault may shallow with depth in a listric sense (Figs. 7B and 7C). However, because pre-rift units (e.g. *Ttsf*) in the footwall of the Kunkaak fault are tilted by a similar amount, the footwall and hanging wall blocks may also have experienced domino-style block tilting. Total dip-slip displacement on the Kunkaak fault is estimated to be ~ 2.8 km, measured on correlative basal *Ttsf* contacts (Fig. 7C), and a minimum of 2.7 km on correlative basement nonconformity surfaces (Fig. 7B).

5.2. Tecomate fault

The Tecomate fault is another significant, north-northwest-striking, west-dipping normal fault exposed in the western part of the study area (Figs. 3, 7B, and 7C). This fault is structurally related to Kunkaak fault, as dip-slip on both structures created tectonic accommodation for Tecomate basin. The Tecomate fault juxtaposes latest Miocene volcanic and sedimentary units (e.g. *Tcg3, Tmr3, Tmr4*) and older Quaternary alluvium (*Qoa*) in the hanging wall against similar units in the footwall, structurally duplicating tilt blocks of Tecomate basin deposits. Fault scarps up to 10 m-high are observed in older Quaternary alluvial deposits (*Qoa*). Oskin (2002) estimated ~3 km of total dip-slip displacement across the Tecomate fault. Along strike to the south, the Tecomate fault serves as the bounding structure between the Sierra Kunkaak and the

Tecomate basin (Fig. 2; Oskin, 2002). Significant dip-slip on the Tecomate fault has led to subsidence of its hanging wall to produce the topographically prominent central valley of Isla Tiburón, Valle de Tecomate.

5.3. Hinzime fault

The Hinzime fault is a normal fault in the Hinzime domain, northeast of the Yawassag fault (Fig. 3). This NNE-striking structure juxtaposes Miocene volcanic units (e.g. *Trhh, Tbhh*) against crystalline basement (*Kt*) and likely dips westward. Total dip-slip displacement on the Hinzime fault is loosely constrained to be ~2.7 km, measured on correlative basement nonconformity surfaces across the fault.

5.4. Yawassag Fault

The Yawassag fault is a first-order, NW-striking, SW-dipping, dextral strike-slip fault that transects the northeastern part of Isla Tiburón and juxtaposes all Neogene map units southwest of the fault against predominantly plutonic rocks northeast of the fault (Fig. 3). The trace of the Yawassag fault is slightly undulatory owing to its moderate (~50°) southwest dip. At one exposure, the fault dips 53° to the southwest with sub-horizontal slickenlines (rake of 011°) (Fig. 3). Prominent, well-exposed, NNW-striking strike-ridges of Tecomate basin deposits (e.g. *Tmr4*, ash marker in *Tcg3*) are deflected in a clockwise sense and are NNE-striking proximal to the dextral Yawassag fault (Fig. 3). The Kunkaak fault and these basin deposits are both truncated by the Yawassag fault and not observed northeast of the fault. Despite its moderate dip, slickenline orientations and clockwise bed deflection of Tecomate basin deposits (e.g., *T3t*, *Tmr4*, and *Tcg3*) immediately adjacent to the fault suggest that dextral strike-slip is the dominant type of

290 motion on the Yawassag fault. Near the northwestern shoreline of this study area, we map
291 a right step in the Yawassag fault, connected by a northwest dipping normal fault (Fig. 3).
292 Late Miocene sedimentary and volcanic units do not correlate across the
293 Yawassag fault. The lack of any correlative Miocene units along the ~8 km onshore
294 exposure of the Yawassag fault, suggests >8 km of dextral displacement has occurred
295 since late Miocene time. This estimate is compatible with published estimates for total
296 dextral shear in the Coastal Sonora fault zone, including 60 ±30 km by Bennett et al.
297 (2013) and ~100 km by Vidal-Solano et al. (2013).
298 Although Gastil and Krummenacher (1977b) considered the Yawassag fault to
299 primarily be a dextral fault, they also considered it to have accommodated significant
300 down-to-the-southwest dip slip. The relatively deeper structural levels of predominantly
301 plutonic rocks exposed in the Hinzime domain northeast of the fault is consistent with
302 this notion (Fig. 3). In contrast, in the Sierra Kunkaak domain southwest of the fault,
303 middle to late Miocene sedimentary and volcanic units are well exposed. The direct
304 association of Tecomate basin subsidence with dextral-oblique motion on the Yawassag
305 fault is unclear; the Yawassag fault may either crosscut and entirely post-date Tecomate
306 basin deposits, or may have been active along the northeastern basin margin during
307 sediment aggradation, as suggested by the subtle thinning (e.g., *Tmr3*) or pinching out
308 (e.g., *Tmr4*) of thick pyroclastic units. If slip on the Yawassag fault was
309 contemporaneous with slip on Kunkaak fault, they may have collectively acted as part of
310 a wrench fault zone.

311 **5.5. Infiernillo Fault**

The Infiernillo fault is a NW-striking, dextral strike-slip fault zone that cuts obliquely through the Tecomate basin (Fig. 3). Bennett et al. (2013) inferred the Infiernillo fault as a strike-slip fault bounding the southwestern edge of the Coastal Sonora fault zone, offshore Bahía de Kino. On northeast Isla Tiburón, the Infiernillo fault cuts and offsets the Kunkaak fault by <1 km of apparent dextral displacement (Fig. 3). The easternmost splay of this zone appears to kinematically link with the Kunkaak fault, where it may have reactivated the Kunkaak fault with dextral-oblique slip. Such reactivation would be responsible for the presence of fault-bounded slivers of *Ttsf* and *Kt* along the Kunkaak fault that are difficult to explain via solely dip-slip motion (Figs. 3 and 7C).

The Infiernillo fault continues towards the northwest where it disrupts and rotates otherwise continuous strike-ridge exposures in the hanging wall of the Kunkaak fault. Farther northwest, the Infiernillo fault merges with the northern end of the Tecomate normal fault in a complex network of normal faults and dextral-oblique normal faults. Recent aeolian deposits (*Qae*) commonly obscure the precise location and connectivity of these faults. Dip-slip displacement on any of these normal faults is unlikely to exceed tens to a few hundred meters.

5.6. Additional Faults and Folds

A NE-striking fault is observed near the southern end of the Tecomate basin and appears to be sub-vertical or may dip steeply to the southeast (Fig. 3). Approximately 200 m of down-to-the-southeast dip-slip motion on this structure may be the cause of the ~500 m apparent dextral offset of Tecomate basin strata here. Three other NE-striking

sinistral faults also cut basin fill rocks in the north-central part of the Tecomate basin, with apparent sinistral displacements of up to ~500m.

A gentle (interlimb angle of ~150°), extension-related syncline is observed in the hanging wall of the Kunkaak fault, immediately west of and parallel to the fault trace (Fig. 3). This syncline deforms deposits of latest Miocene non-marine conglomerate (e.g. *Tcg3*) that overlie the Tuffs of Mesa Cuadrada (Figs. 7B and 7C). The axial plane trace of this syncline displays ~100 m of apparent sinistral displacement along a NE-striking strike-slip fault (Fig. 3).

6. TIMING OF FAULTING AND BASIN FORMATION

Integration of structural and stratigraphic relationships with new and previously published geochronologic age constraints permits us to estimate the timing of transtensional faulting and related basin formation on northeastern Isla Tiburón. We interpret that Tecomate basin deposits accumulated in response to tectonic subsidence formed by activity on the Kunkaak and Tecomate normal faults. Thus, Tecomate basin deposits directly constrain the timing of slip on these normal faults. The Tecomate basin appears to be wedge-shaped, with zero to a few tens of meters of pre-6.4 Ma (*Tmr3*) deposits near its southern end (Fig. 3), but thickens to 1.2 ± 0.1 km of pre-6.4 Ma deposits along strike to the north (Figs. 7B and 7C). This basin geometry may be interpreted to suggest that the slip rate of the Kunkaak fault was higher towards its northern end, or that slip initiated earlier to the north and propagated southward. Alternatively, the basin may have also been slightly tilted northward so that sediments accumulated in the northern part of the basin first.

The tilting rate between isotopically dated tuffs, interbedded within the Tecomate basin, can be used to estimate the onset of normal fault activity and the age of the oldest basin deposits. A continuous and relatively unfaulted transect of the Tecomate basin occurs along cross section C-C' (Fig. 7C). Here, Tecomate basin deposits display a continuous, up-section fanning-dip geometry, indicative of its syn-tectonic association with the Kunkaak fault. The 7.1 Ma Tecomate ash bed is inclined ~50°, while the 6.4 Ma Tuffs of Mesa Cuadrada (*Tmr3*) is inclined ~25°, yielding a tilting rate of ~36°/Myr. The middle Miocene units that underlie the Tecomate basin are inclined ~60–75°. If a constant tilting rate is assumed, we estimate that slip on the Kunkaak fault and related horizontal-axis block tilting and basin subsidence in its hanging wall commenced 7.6 ± 0.2 Ma. However, if the rate of tilting was initially slower, then the age of onset of fault slip could be older.

The sedimentation rate between these intra-basin tuffs can also be used to estimate the age of the oldest basin deposits. From structural cross section C-C' (Fig. 7C), we estimate stratigraphic thicknesses at depth, adjacent to the Kunkaak fault, where the thickest section of the Tecomate basin occurs. Here, we estimate 1000 m of basin deposits exist between the 7.1 Ma Tecomate ash bed and the basal contact of the 6.4 Ma Tuffs of Mesa Cuadrada (*Tmr3*), yielding a sedimentation rate of ~1.4 mm/yr. Approximately 400 m of conglomerate and sandstone occur stratigraphically below the 7.1 Ma Tecomate ash bed. Again, if a constant sedimentation rate were assumed, we estimate that the oldest non-marine sedimentary deposits in the Tecomate basin are ca. 7.4 Ma, similar to our age estimate determined from the block-tilting rate.

379 Crosscutting relationships between structures and isotopically-dated basin
380 deposits (Fig. 3) also provide timing information for activity of dextral faults. Latest
381 Miocene Tecomate basin deposits, the Kunkaak fault, and extension-related folds are all
382 crosscut and truncated by the dextral-oblique Yawassag fault. These relationships suggest
383 that significant activity on the Yawassag fault must post date 6.4 Ma. However, because
384 no Tertiary units correlate across the Yawassag fault, pre-7 Ma activity cannot be ruled
385 out. The Infiernillo fault cuts obliquely through the core of the Tecomate basin and
386 offsets tilted strike ridges of resistant units (e.g., the 6.4 Ma Tuffs of Mesa Cuadrada)
387 without significant change in the strike or dip of these laterally continuous units (Figs. 3,
388 7B, and 7C), suggesting that dextral offset occurred after the units were tilted. Also, we
389 do not observe changes in basin thickness across splays of the Infiernillo fault, indicating
390 that they did not control basin depositional patterns and may have not yet been
391 established. These observations suggest that activity on the Infiernillo fault likely
392 initiated sometime after 6.4 Ma, after deposition and tilting of the Tecomate basin
393 deposits.

394 Paleomagnetic data also provide timing information about dextral shear on
395 northeastern Isla Tiburón. Paleomagnetic results indicate that ~70% of the total ~29° of
396 clockwise vertical-axis block rotation in the Sierra Kunkaak domain occurred after
397 emplacement of the 12.5 Ma Tuff of San Felipe and prior to emplacement of the 6.4 Ma
398 Tuffs of Mesa Cuadrada (Bennett and Oskin, 2014), suggesting that a form of dextral
399 deformation was active prior to 6.4 Ma. If the rate of clockwise rotation was initially
400 slow, the onset of dextral shear could be older and could have initiated any time after
401 ~12.5 Ma, possibly due to dextral faulting outside of the study area. Alternatively, if this

dextral deformation initiated concurrent with the onset of normal faulting, it may have also begun ca. 7.6 ± 0.2 Ma.

No undeformed units cap faults and related basin deposits on northeastern Isla Tiburón that can be used to constrain the cessation of fault activity. However, post-6.4 Ma Tecomate basin deposits are gradually less inclined up-section (Figs. 3, 7B, and 7C), indicating that normal fault activity continued for some time after 6.4 Ma. Likewise, a portion of dextral fault slip must post-date the 6.4 Ma Tuffs of Mesa Cuadrada, which are crosscut by dextral faults and experienced ~8° of clockwise vertical-axis rotation (Bennett and Oskin, 2014).

7. REGIONAL IMPLICATIONS

7.1. Relationship to the Coastal Sonora Fault Zone

7.1.1. Timing and Style of Onshore Faulting

Coastal Sonora and northeastern Isla Tiburón share a similar history of transtensional faulting, clockwise vertical-axis block rotations, and syn-tectonic basin formation. Thus we interpret faults exposed on northeastern Isla Tiburón to be components of the Coastal Sonora fault zone. Specifically, the Sacrificio fault in coastal Sonora projects offshore to the northwest, across the Canal de Infiernillo, and is aligned with the Yawassag fault onshore northeastern Isla Tiburón. The offshore Infiernillo fault, inferred to parallel the Sonoran coastline between Bahía de Kino and Punta Chueca, also projects across the Canal de Infiernillo. Collectively, these structures bound the Coastal Sonora fault zone, which was a zone of significant transtensional deformation during latest Miocene time (Bennett et al., 2013; this study).

Although we cannot confidently estimate the onset of deformation, similar to the Bennett et al. (2013) study, the sedimentary record of syn-tectonic tilting on northeastern Isla Tiburón and clockwise block rotation is comparable with the record from coastal Sonora. On the Sonora mainland, 30–50 km along strike to the southeast of northeastern Isla Tiburón, syn-tectonic basin-fill accumulation and clockwise vertical-axis block rotation commenced sometime after 11.5 Ma, with the majority of fault-related basin subsidence and tectonic tilting occurring after 8–7 Ma (Bennett et al., 2013). The tilted and rotated deposits in the Kino basin in coastal Sonora were subsequently cut and dextrally offset by NW-striking dextral faults (Bennett et al., 2013), while this late-stage dextral shear was accommodated by further clockwise vertical-axis rotation of the Punta Chueca basin (Bennett et al., 2013; Bennett and Oskin, 2014). A similar sequence of events appears to have affected northeastern Isla Tiburón, where deposits of the Tecomate basin of were first tilted and rotated clockwise, then were subsequently crosscut by strike-slip faults during additional clockwise rotation. Tilting rates of pre-6.4 Ma Tecomate basin deposits (~36°/Myr) are similar to pre-6.4 Ma tilting rates in the Punta Chueca basin (~47°/Myr). Sedimentation rates in the Tecomate basin (~1.4 mm/yr) are also similar to the Punta Chueca basin (1.2 ± 0.2 mm/yr) for a similar interval.

7.1.2. Timing and Style of Offshore Faulting

The Coastal Sonora fault zone on northeastern Isla Tiburón continues to the northwest and is likely related to normal faults (e.g., Desemboque fault) and dextral strike-slip faults (e.g., De Mar fault) observed in offshore geophysical lines. These offshore faults were the primary structures that accommodated the oblique opening of the Upper Tiburón pull-apart basin (Lonsdale, 1989; González-Fernández et al., 2005; Mar-

448 Hernandez et al., 2012) and control the irregular, right-stepping geometry of the
449 submerged rifted margin of the North American plate (Mar-Hernandez et al., 2012).
450 Because the Lower Tiburón basin did not open until after 6.4–6.1 Ma (Oskin and Stock,
451 2003a), possibly only the waning phases (latest Miocene–early Pliocene(?)) of dextral
452 slip across the Coastal Sonora fault zone may have been coeval with, and kinematically
453 linked to these offshore structures. As onshore structures related to the Coastal Sonora
454 fault zone became inactive, the oblique extension that previously occurred in the region
455 between the Coastal Sonora fault zone and the La Cruz-Tiburón transform migrated west
456 of Isla Tiburón, initiating oblique opening of the Upper Tiburón basin. This westward
457 jump in the locus of transtensional deformation and pull-apart basin formation is similar
458 to the documented ca. 3 Ma westward jump of deformation from the Upper Tiburón basin
459 to the Upper Delfín basin (Aragon-Areola and Martín-Barajas, 2007), but is an
460 additional, older step in the evolution of this rift segment of the Pacific-North America
461 plate boundary.

462 **7.2. Relationship to the Faulting in Northeastern Baja California**

463 Transtensional fault systems documented in northeastern Baja California (e.g.,
464 Seiler et al., 2010) may have once been additional components of the Coastal Sonora
465 fault zone. Upon palinspastic restoration of the oblique opening of the Gulf of California
466 and restoration of Baja California ~250 km towards the southeast (e.g., Oskin and Stock,
467 2003a), the San Felipe region of Baja California aligns with the northwestward projection
468 of the Coastal Sonora fault zone. Approximately 8 km west of the coastal town of San
469 Felipe, Seiler et al. (2010) mapped an unnamed, NW-striking dextral fault zone that may
470 be kinematically linked to the Santa Rosa detachment fault. This unnamed dextral fault

zone may have once been the northwestward continuation of dextral faults on the Coastal Sonora fault zone, such as the Yawassag fault.

Rift-related normal faults in northeastern Baja California appear to have developed as mirror images of normal faults in coastal Sonora and their related syn-tectonic basins seem to share an identical timing history. For example, major normal and detachment faults in Baja California are southeast or east dipping (Seiler et al., 2010), whereas normal and detachment faults in coastal Sonora and northeastern Isla Tiburón are northwest or west dipping (Bennett et al., 2013; this study). Correspondingly, syn-tectonic basins in Baja California (e.g., Santa Rosa, Huatamote, and Llano El Moreno basins) are inclined down-to-the-northwest or -west and basins in coastal Sonora (e.g., Kino and Punta Chueca basins) and on northeastern Isla Tiburón (e.g., Tecomate basin) are inclined down-to-the-southeast or -east. The latest Miocene onset of transtensional faulting and basin formation on northeastern Baja California (9–7 Ma; Seiler et al., 2010) is similar to the 8–7 Ma onset documented in coastal Sonora (8–7 Ma; Bennett et al., 2013) and northeastern Isla Tiburón (this study).

8. SUMMARY AND CONCLUSIONS

This study documents the development and activity of latest Miocene transtensional faulting in the Coastal Sonora fault zone on northeastern Isla Tiburón. Transtensional tectonics formed the syn-tectonic Tecomate basin, which accumulated non-marine sedimentary and pyroclastic deposits proximal to, and immediately before the formation of, the eastern, rifted margin of the Gulf of California (North America plate). Detailed structural and geologic mapping documents the intersection and crosscutting

494 relationships of several significant rift-related fault systems (e.g., Kunkaak, Tecomate,
495 Hinzime, Infiernillo, and Yawassag faults) and the crosscutting relationships of these
496 structures with Tecomate basin deposits.

497 From extrapolation of sedimentation and tilting rates to the base of the Tecomate
498 basin, normal faulting related to transtensional rifting is estimated to have initiated ca. 7.6
499 ± 0.2 Ma on the Kunkaak fault. During the 7.1–6.4 Ma interval, non-marine sandstone
500 and conglomerate accumulated at ~1.4 mm/yr above a half-graben structurally related to
501 the Kunkaak fault, which tilted ~36°/Myr. At least 1.8 ± 0.1 km of sediments
502 accumulated in the Tecomate basin as ~2.8 km of total dip-slip motion occurred on the
503 Kunkaak normal fault. Approximately 70% of the total ~29° of clockwise vertical-axis
504 block rotation in the Sierra Kunkaak domain occurred sometime between 12.5 Ma and
505 6.4 Ma. An angular unconformity (up to ~20° of discordance) exists between middle
506 Miocene volcanic rocks and the oldest exposed Tecomate basin deposits. These basin
507 deposits were tilted and rotated clockwise, then were subsequently crosscut by strike-slip
508 faults during additional clockwise rotation. These timing constraints are almost identical
509 to the Coastal Sonora fault zone, along strike to the southeast near Bahía de Kino and
510 Punta Chueca, where the majority of rapid transtensional faulting occurred between ca. 8
511 Ma and 6–5 Ma (Bennett et al., 2013).

512 Latest Miocene transtensional deformation in the Coastal Sonora fault zone on
513 northeastern Isla Tiburón was related to the development of the Gulf of California Shear
514 Zone (Bennett and Oskin, 2014), a narrow NNW-trending belt of localized strike-slip
515 faulting, clockwise block rotation, and subsiding pull-apart basins that formed coincident
516 with an increase in rift obliquity ca. 8 Ma (Atwater and Stock, 1998; Atwater and Stock,

2013). Rapid transtensional deformation in coastal Sonora is synchronous with the 8–7 Ma onset of transform faulting and basin formation along the nascent PAC-NAM plate boundary in northwest Mexico and southern California (Bennett et al., 2016). Although PAC-NAM oblique rifting initiated ca. 12.3 Ma (Atwater and Stock, 1998), the development of major strike-slip faults appears to have been delayed for several million years, until ca. 9–8 Ma (e.g., Seiler et al., 2010; Bennett et al., 2013; Bennett et al., 2016; this study). Once the Gulf of California shear zone materialized along much of the PAC-NAM plate boundary in northwestern México, it facilitated the localization of plate boundary strain (Oskin et al., 2001; Oskin and Stock, 2003a) and subsequently catalyzed continental rupture in the Gulf of California.

ACKNOWLEGMENTS

Funding from the National Science Foundation Tectonics and MARGINS programs (awards #0739017 and #0904337), an ExxonMobil Geoscience Grant, a Geological Society of America Graduate Student Research Grant, a Northern California Geological Society Richard Chambers Memorial Scholarship, and a UC Davis Cordell Durrell scholarship made this research possible. Permission to enter Isla Tiburón was granted by the Secretaría de Medio Ambiente y Recursos Naturales-Comisión Nacional de Areas Naturales Protegidas and the native Cumcaác (Seri) tribe. We thank A. Martín-Barajas for assistance with permit acquisition. Reviews by XX and XX helped improve the manuscript. M. Tappa, E. Stevens, and J. Ford all provided great company, safety, and support while conducting fieldwork on northeastern Isla Tiburón. We thank the Molina Villa-Lobos family (Ernesto, Francisco, and Esequel) of the of the native Cumcaác (Seri) tribe for their transportation support and safekeeping during our field research.

FIGURE CAPTIONS

Figure 1

Physiographic map of the northern Gulf of California. Structures related to oblique rifting shown from Fenby and Gastil (1991), Oskin (2002), Aragón-Arreola & Martín-Barajas (2007), Aragón-Arreola et al. (2005), Seiler et al. (2010), Pacheco et al. (2006), Mar-Hernández et al. (2012), Bennett et al. (2013), Darin et al. (2016), Bennett et al., 2016, this study. Active Pacific-North America plate boundary structures colored in red. Inactive structures related to early oblique rifting colored black. Rhomboid-shaped transtensional pull-apart basins (white lines) from Aragón-Arreola and Martín-Barajas (2007) and Lonsdale (1989). Cross-gulf tie points include 'F'–fusulinid-rich clast conglomerate (Gastil et al., 1973), and widespread tuffs shown in red and green (Oskin et al., 2001; Oskin and Stock, 2003a). Vent locations for widespread tuffs shown with stars. (INSET MAP) Simplified regional tectonic map of Western North America showing the diffuse boundary between the Pacific-North American lithospheric plates (after Oskin and Stock, 2003a). Active faults and spreading centers in red. Stable continental blocks in gray. Extensional provinces in tan.

Figure 2

Simplified geologic map of Isla Tiburón and coastal Sonora. Schematic stratigraphic column of geology units shown. Geology compiled from Gastil and Krummenacher (1977a), Oskin, (2002), Bennett et al. (2013), Bennett et al., (2016) this study. See Figure 3 legend for description of fault symbology.

Figure 3

1: 15,000-scale geologic map of northeastern Isla Tiburón. New and previously published geochronologic sample locations and isotopic ages are shown on map. All stratigraphic and structural data are displayed on the large geologic map. Printed map sheet is 42" tall, 36" wide.

Figure 4

Schematic stratigraphic columns of geologic map units for northeastern Isla Tiburón. Lithologic unit indicators and colors correspond to units on geologic map (Fig. 3) and geologic cross sections (Fig. 7). Isotopic ages (in million years) for units are shown in parentheses. See text for descriptions of map units and details of isotopic ages.

Figure 5

$^{40}Ar/^{39}Ar$ geochronologic ages calculated for the Tecomate ash bed, which is interbedded low in the Tecomate basin on northeastern Isla Tiburón. (A) $\%^{40}Ar^*$, K/Ca ratios, and ranked age plot of multiple, single-grain, total fusion ages on potassium-feldspar (sanidine) crystals (left) and inverse-isotope correlation diagram (right). (B) Identical plots as (A) for multiple, single-grain, total fusion ages on plagioclase crystals from same sample. Crystals omitted from mean age calculation are gray hollow circles (left) and gray shaded ellipses and crystal numbers (right). This is the same sample dated with $^{206}Pb/^{238}U$ techniques (Fig. 6). See Table 1 for analytical data.

Figure 6

$^{206}Pb/^{238}U$ Tera-Wasserburg concordia diagram (left panels), relative probability age diagram (upper right), and ranked age plot (lower right) for multiple zircon crystals from samples of the Tecomate ash bed, interbedded low in the Tecomate basin on northeastern Isla Tiburón. Black arrow indicates mean age on ranked age plot. Zircon crystals omitted from mean age calculation are gray squares with gray, dashed error ellipses. Relatively younger zircons have high uranium concentrations (Table 2) and are omitted from mean age due to possible lead loss. Relatively older zircons are omitted due to potential inheritance. This is the same sample dated with $^{40}Ar/^{39}Ar$ techniques (Fig. 5). See Table 2 for analytical data.

Figure 7

Geologic cross-sections across northeastern Isla Tiburón. (A) Cross-section across the Hinzime domain, northeast of the Yawassag fault. (B) Cross-section across the northern Tecomate basin. (C) Cross-section across the southern Tecomate basin. Map unit lithologic indicators, colors, and other symbology as in Figures 3 and 4. Dip values from structural measurements used to construct cross-sections shown near ground surface. Apparent dip values shown in parentheses. See geologic map (Fig. 3) for cross-section line locations.

609 **REFERENCES CITED**

610 Andersen, T., 2002, Correction of common lead in U-Pb analyses that do not report Pb-
611 204: Chemical Geology, v. 192, no. 1-2, p. 59-79.
612 Aragón-Arreola, M., and Martín-Barajas, A., 2007, Westward migration of extension in
613 the northern Gulf of California, Mexico: Geology, v. 35, no. 6, p. 571-574.
614 Aragón-Arreola, M., Morandi, M., Martín-Barajas, A., Deldago-Argote, L., and
615 González-Fernández, A., 2005, Structure of the rift basins in the central Gulf of
616 California: Kinematic implications for oblique rifting: Tectonophysics, v. 409, p. 19-
617 38.
618 Atwater, T., and Stock, J., Constraints on the history of the Late Cenozoic Pacific-North
619 American plate boundary from marine magnetic anomalies and global plate circuits,
620 in Proceedings Geological Society of America Cordilleran Section - 109th Annual
621 Meeting, Fresno, CA, 2013, Volume 45, p. 21.
622 Atwater, T., and Stock, J. M., 1998, Pacific North America plate tectonics of the Neogene
623 southwestern United States: An update: International Geology Review, v. 40, no. 5,
624 p. 375-402.
625 Bennett, S.E.K., 2009, Transtensional rifting in the late proto-Gulf of California near
626 Bahía Kino, Sonora, México [M.S. thesis]: University of North Carolina, Chapel
627 Hill, 122 p.
628 Bennett, S.E.K., Oskin, M.E., and Iriondo, A., 2013, Transtensional rifting in the proto-
629 Gulf of California, near Bahía Kino, Sonora, México: Geological Society of America
630 Bulletin, v. 125, p. 1752–1782, doi: 10 .1130 /B30676 .1

631 Bennett, S. E. K., and Oskin, M. E., 2014, Oblique rifting ruptures continents: Example
632 from the Gulf of California shear zone: Geology, v. 42, no. 3, p. 215-218.
633 Bennett, S.E.K., Oskin, M.E., Dorsey, R.J., Iriondo, A., and Kunk, M.J., 2015,
634 Stratigraphy and structural development of the southwest Isla Tiburón marine basin:
635 Implications for latest Miocene tectonic opening and flooding of the northern Gulf of
636 California, Geosphere, GES01153-1.
637 Bennett, S.E.K., Oskin, M.E., Iriondo, A., and Kunk, M.J., 2016, Slip history of the La
638 Cruz fault: development of a late Miocene transform in response to increased rift
639 obliquity in the northern Gulf of California, Tectonophysics (waiting on
640 volume/page # information)
641 Darin, M. H., Dorsey, R. J., Bennett, S. E. K., Oskin, M. E., Iriondo, A., and Kunk, M. J.,
642 2016, Late Miocene Extension in Coastal Sonora, México: Implications for the
643 Evolution of Dextral Shear in the Proto-Gulf of California Oblique Rift:
644 Tectonophysics (waiting on volume/page # information)
645
646 Dorsey, R. J., Housen, B. A., Janecke, S. U., Fanning, C. M., and Spears, A. L. F., 2011,
647 Stratigraphic record of basin development within the San Andreas fault system: Late
648 Cenozoic Fish Creek-Vallecito basin, southern California: Geological Society of
649 America Bulletin, v. 123, no. 5-6, p. 771-793.
650 Fenby, S. S., and Gastil, R. G., 1991, Geologic-Tectonic Map of the Gulf of California
651 and Surrounding Areas, in Dauphin, J. P., and Simoneit, B. R. T., eds., AAPG
652 Memoir 47: The Gulf and Peninsular Province of the Californias, Volume 47, p. 79-
653 83.

654 Gans, P. B., 1997, Large-magnitude Oligo-Miocene extension in southern Sonora:
655 Implications for the tectonic evolution of northwest Mexico: Tectonics, v. 16, no. 3,
656 p. 388-408.
657 Gastil, R. G., and Krummenacher, D., 1977a, Reconnaissance geologic map of coastal
658 Sonora between Puerto Lobos and Bahia Kino, GSA Map and Chart Series MC-16:
659 Geological Society of America, scale 1:150,000.
660 -, 1977b, Reconnaissance geology of coastal Sonora between Puerto Lobos and Bahia
661 Kino: Geological Society of America Bulletin, v. 88, no. 2, p. 189-198.
662 Gastil, R. G., Lemone, D. V., and Stewart, W. J., 1973, Permian fusulinids from near San
663 Felipe, Baja California: American Association of Petroleum Geologists Bulletin, v.
664 57, no. 4, p. 746-747.
665 González-Fernández , A., Danobeitia, J. J., Deldago-Argote, L., Michaud, F., Cordoba,
666 D., and Bartolome, R., 2005, Mode of extension and rifting history of upper Tiburon
667 and upper Delfin basins, northern Gulf of California: Journal of Geophysical
668 Research, v. 110, p. 1-17.
669 Larson, R. L., Menard, H. W., and Smith, S. M., 1968, Gulf of California: a result of
670 ocean floor spreading and transform faulting: Science, v. 161, p. 781-784.
671 Lewis, C. J., 1996, Stratigraphy and geochronology of Miocene and Pliocene volcanic
672 rocks in the Sierra San Fermín and southern Sierra San Felipe, Baja California,
673 Mexico: Geofisica Internacional, v. 35, p. 1-31.
674 Lizarralde, D., Axen, G. J., Brown, H. E., Fletcher, J. M., González-Fernández, A.,
675 Harding, A. J., Holbrook, W. S., Kent, G. M., Paramo, P., Sutherland, F., and

676 Umhoefer, P. J., 2007, Variation in styles of rifting in the Gulf of California: Nature,
677 v. 448, p. 466-469.
678 Lonsdale, P., 1989, Geology and tectonic history of the Gulf of California, in Winterer,
679 E. L., Hussong, D. M., and Decker, R. W., eds., The Eastern Pacific Ocean and
680 Hawaii, Geology of North America, Volume N: Boulder, CO, Geological Society of
681 America, p. 499-521.
682 Ludwig, K. R., 2003, Mathematical-statistical treatment of data and errors for Th-230/U
683 geochronology: Uranium-Series Geochemistry, v. 52, p. 631-656.
684 Mar-Hernández, E., González-Escobar, M., and Martín-Barajas, A., 2012, Tectonic
685 framework of Tiburon Basin, Gulf of California, from seismic reflection evidence:
686 International Geology Review, v. 54, no. 11, p. 1271-1283.
687 Martín-Barajas, A., González-Escobar, M., Fletcher, J. M., Pacheco, M., Oskin, M., and
688 Dorsey, R., 2013, Thick deltaic sedimentation and detachment faulting delay the
689 onset of continental rupture in the Northern Gulf of California: Analysis of seismic
690 reflection profiles: Tectonics, v. 32, p. 18.
691 Nagy, E. A., Grove, M., and Stock, J. M., 1999, Age and stratigraphic relationships of
692 pre- and syn-rift volcanic deposits in the northern Puertecitos Volcanic Province,
693 Baja California, Mexico: Journal of Volcanology and Geothermal Research, v. 93, p.
694 1-30.
695 Nicholson, C., Sorlien, C. C., Atwater, T., Crowell, J. C., and Luyendyk, B. P., 1994,
696 Microplate capture, rotation of the western Transverse Ranges, and initiation of the
697 San Andreas transform as a low-angle fault system: Geology, v. 22, p. 491-495.

698 Niño-Estrada, L., Iriondo, A., García-Flores, R., McDowell, F. W., Izaguirre, A., Bennett,
699 S. E. K., and Oskin, M. E., Edades Cretácicas de rocas batolíticas del Isla Tiburón,
700 Golfo de California: Geocrhonología U-Pb en zircones mediante técnicas de
701 ablación láser e ICP-MS, in Proceedings Unión Geofísica Mexicana Reunión Anual,
702 Puerto Vallarta, Mexico, 2014.
703 Oskin, M., 2002, Tectonic Evolution of The Northern Gulf of California, Mexico,
704 Deduced from Conjugate Rifted Margins of the Upper Delfín BasinPh.D.]:
705 California Institute of Technology, 481 p.
706 Oskin, M., Stock, J., and Martín-Barajas, A., 2001, Rapid localization of Pacific-North
707 America plate motion in the Gulf of California: Geology, v. 29, no. 5, p. 459-462.
708 Oskin, M., and Stock, J. M., 2003a, Pacific-North America plate motion and opening of
709 the Upper Delfín basin, northern Gulf of California: Geological Society of America
710 Bulletin, v. 115, p. 1173–1190.
711 -, 2003b, Marine incursion synchronous with plate-boundary localization in the Gulf of
712 California: Geology, v. 31, p. 23-26.
713 Oskin, M., and Martín-Barajas, A., 2003, Continental edge tectonics of Isla Tiburón,
714 Sonora Mexico, in Alcayde, M., and Caballero, A. G., eds., Geological Transects
715 Across Cordilleran Mexico, Volume 1: Mexico, D.F., Universidad Nacional
716 Autónoma de México, p. 53-70.
717 Pacheco, M., Martín-Barajas, A., Elders, W., Espinosa-Cardena, J. M., Helenes, J., and
718 Segura, A., 2006, Stratigraphy and structure of the Altar basin of NW Sonora:
719 Implications for the history of the Colorado River delta and the Salton trough:
720 Revista Mexicana de Ciencias Geologicas, v. 23, no. 1, p. 22.

721 Schaaf, P., Roldan-Quintana, J., and Calmus, T., 1999,Terrane Reconnaissance in NE
722 Sonora, Mexico, in the Light of Sr-Nd-Pb Isotopic Data From Coastal Belt
723 Granitoids, in Proceedings AGU Fall Meeting.
724 Seiler, C., Fletcher, J. M., Quigley, M. C., Gleadow, A. J. W., and Kohn, B. P., 2010,
725 Neogene structural evolution of the Sierra San Felipe, Baja California: Evidence for
726 proto-Gulf transtension in the Gulf Extensional Province?: Tectonophysics, v. 488,
727 p. 87-109.
728 Simon, J. I., Renne, P. R., and Mundil, R., 2008, Implications of pre-eruptive magmatic
729 histories of zircons for U-Pb geochronology of silicic extrusions: Earth and
730 Planetary Science Letters, v. 266, no. 1-2, p. 182-194.
731 Sláma, J., Kosler, J., Condon, D. J., Crowley, J. L., Gerdes, A., Hanchar, J. M.,
732 Horstwood, M. S. A., Morris, G. A., Nasdala, L., Norberg, N., Schaltegger, U.,
733 Schoene, B., Tubrett, M. N., and Whitehouse, M. J., 2008, Plesovice zircon - A new
734 natural reference material for U-Pb and Hf isotopic microanalysis: Chemical
735 Geology, v. 249, no. 1-2, p. 1-35.
736 Spencer, J.E., and Normark, W.R., 1979, Tosco-Abreojos fault zone: A Neogene
737 transform plate boundary within the Pacific margin of southern Baja California,
738 Mexico, Geology v. 7, no. 11, p. 554-557.
739 Stock, J. M., 1989, Sequence and geochronology of Miocene rocks adjacent to the main
740 gulf escarpment: Southern Valle Chico, Baja California Norte, Mexico: Geofisica
741 Internacional, v. 28, no. 5, p. 851-896.

742 Stock, J. M., Lewis, C. J., and Nagy, E. A., 1999, The Tuff of San Felipe: an extensive
743 middle Miocene pyroclastic flow deposit in Baja California, Mexico: Journal of
744 Volcanology and Geothermal Research, v. 93, p. 53-74.
745 Stock, J. M., and Molnar, P., 1988, Uncertainties and implications of the Late Cretaceous
746 and Tertiary position of North America relative to the Farallon, Kula, and Pacific
747 plates: Tectonics, v. 7, no. 6, p. 1339-1384.
748 Umhoefer, P. J., 2011, Why did the Southern Gulf of California rupture so rapidly?—
749 Oblique divergence across hot, weak lithosphere along a tectonically active margin:
750 GSA Today, p. 4-10.
751 Vidal-Solano, J. R., Lozano Santa Cruz, R., Zamora, O., Mendoza-Cordova, A., and
752 Stock, J. M., 2013, Geochemistry of the extensive peralkaline pyroclastic flow
753 deposit of NW Mexico, based on conventional and handheld X-ray fluorescence.
754 Implications in a regional context: Journal of Iberian Geology, v. 39, no. 1, p. 121-
755 130.
756

Table 1 $^{40}Ar/^{39}Ar$ laser total fusion data of single-crystal k-feldspar ang plagioclase crystals from Tecomate ash bed or

Hole number	$^{39}Ar_k$ (Moles)	Radiogenic Yield (%)	$^{40}Ar^*/^{39}Ar_k$	K/Ca	K/Cl	Age (Ma)	Error (Ma)
TIB-09-25	*Sonora, Mexico*	***sanidine***	*J = 0.004398 ± 0.25%*		*#190KD53*		
3	1.18E-14	95.8	0.870	59.7	4000	**6.89**	**± 0.03**
29	3.21E-15	97.1	0.881	74.9	14286	**6.98**	**± 0.07**
31	5.26E-15	96.7	0.882	55.6	33333	**6.98**	**± 0.03**
7	8.80E-15	96.3	0.886	62.5	7692	**7.02**	**± 0.04**
4	7.40E-15	83.3	0.891	66.1	8333	**7.05**	**± 0.05**
37	4.46E-15	91.4	0.892	52.8	10000	**7.07**	**± 0.05**
19	4.62E-15	97.0	0.897	79.3	5556	**7.10**	**± 0.04**
11	8.63E-15	91.2	0.898	67.3	10000	**7.11**	**± 0.04**
13	8.86E-15	99.4	0.899	81.3	8333	**7.12**	**± 0.02**
12	9.04E-15	95.7	0.901	50.5	5556	**7.13**	**± 0.04**
20	9.65E-15	99.1	0.903	79.4	***	**7.15**	**± 0.03**
40	4.01E-15	98.9	0.904	57.3	9091	**7.15**	**± 0.05**
30	2.64E-15	99.3	0.904	34.7	4545	**7.16**	**± 0.07**
2	9.82E-15	99.8	0.907	87.3	0	**7.18**	**± 0.03**
18	7.45E-15	99.1	0.908	152.9	11111	**7.19**	**± 0.03**
38	6.62E-15	98.3	0.908	188.7	25000	**7.19**	**± 0.03**
6	1.01E-14	96.7	0.911	70.9	2273	**7.21**	**± 0.03**
41	1.40E-15	89.3	0.926	104.4	12500	**7.33**	**± 0.14**
22	8.21E-15	97.5	1.465	73.8	5556	11.59	± 0.03
		MSWD = 3.46		**Weighted Mean Age =**		**7.11**	**± 0.09**
TIB-09-25	*Sonora, Mexico*	***plagioclase***	*J = 0.004398 ± 0.25%*		*#190KD53*		
28	5.70E-16	67.4	0.751	0.6	***	**5.95**	**± 0.31**
5	1.35E-15	77.6	0.799	0.6	5263	**6.33**	**± 0.27**
24	6.75E-16	57.7	0.801	0.8	2778	**6.34**	**± 0.29**
9	1.16E-15	58.9	0.804	0.6	2857	**6.37**	**± 0.26**
8	9.78E-16	74.7	0.810	0.7	3846	**6.42**	**± 0.31**
10	2.74E-15	46.1	0.820	1.5	2941	**6.49**	**± 0.15**
26	6.82E-16	81.1	0.825	0.6	***	**6.53**	**± 0.26**
25	9.62E-16	83.0	0.838	0.6	***	**6.63**	**± 0.19**
15	7.72E-16	87.4	0.847	0.8	***	**6.71**	**± 0.25**
14	1.59E-15	88.6	0.857	0.9	3125	**6.79**	**± 0.15**
36	9.24E-16	80.6	0.872	0.5	3846	**6.90**	**± 0.21**
17	1.08E-15	91.4	0.883	0.7	2703	**6.99**	**± 0.18**
27	1.08E-15	67.8	0.883	0.6	1299	**6.99**	**± 0.23**
21	1.24E-15	83.2	0.889	0.5	***	**7.04**	**± 0.16**
42	8.77E-16	97.9	0.918	0.6	2632	**7.27**	**± 0.22**
23	6.51E-16	89.8	0.951	0.4	6250	**7.53**	**± 0.28**
34	5.72E-16	94.3	0.963	0.6	8333	**7.63**	**± 0.31**
16	9.03E-16	100.0	0.964	0.4	***	**7.63**	**± 0.20**
33	6.26E-16	88.3	0.972	0.8	2703	**7.69**	**± 0.27**
32	1.06E-15	87.9	0.983	0.6	6667	**7.79**	**± 0.18**
1	7.34E-16	66.5	0.993	0.8	1587	**7.86**	**± 0.42**
39	5.62E-16	100.0	1.047	0.5	2273	**8.29**	**± 0.33**
35	4.97E-16	100.0	1.049	0.8	4000	**8.30**	**± 0.35**
		MSWD = 5.93		**Weighted Mean Age =**		**7.00**	**± 0.50**

Analyses in gray italics are not used to calculate the weighted mean age

Table 2 U-Th-Pb analytical data for LA-ICPMS spot analyses on zircon crystals from Tecomate ash bed on northeastern Isla Tiburón.

				CORRECTED RATIOS										CORRECTED AGES (Ma)									
	$U^{\#}$ (ppm)	$Th^{\#}$ (ppm)	Th/U	$^{207}Pb/^{206}Pb^{\dagger}$	±1s*	$^{207}Pb/^{235}U^{\dagger}$	±1s*	$^{206}Pb/^{238}U^{\dagger}$	±1s*	$^{208}Pb/^{232}Th^{\dagger}$	±1s*	Rho	% disc**	$^{206}Pb/^{238}U$	±1s*	$^{207}Pb/^{235}U$	±1s*	$^{207}Pb/^{206}Pb$	±1s*	$^{208}Pb/^{232}Th$	±1s*	Best age (Ma)	1s
Sample **TIB-09-25**		Mount ICGEO-7 (October 2009)																					
TIB25-**27**	1551	752	0.45	0.0476	0.0018	0.0063	0.0003	0.0010	0.00001	0.0003	0.00001	0.240	3	6.2	0.1	6.4	0.3	81	84	6.2	0.2	6.2 ±	0.1
TIB25-**8**	1122	591	0.48	0.0586	0.0031	0.0078	0.0004	0.0010	0.00001	0.0003	0.00001	0.250	20	6.3	0.1	7.9	0.4	554	113	6.5	0.2	6.3 ±	0.1
TIB25-**23**	1160	397	0.31	0.0462	0.0016	0.0064	0.0002	0.0010	0.00001	0.0003	0.00002	0.200	2	6.4	0.1	6.5	0.2	9	68	6.8	0.5	6.4 ±	0.1
TIB25-**19**	626	503	0.74	0.0531	0.0043	0.0078	0.0007	0.0011	0.00002	0.0003	0.00001	0.210	13	6.9	0.1	7.9	0.7	331	181	6.8	0.2	**6.9 ±**	**0.1**
TIB25-**11**	609	147	0.22	0.0504	0.0029	0.0075	0.0005	0.0011	0.00002	0.0003	0.00001	0.270	8	7.0	0.1	7.6	0.5	212	129	6.9	0.2	**7.0 ±**	**0.1**
TIB25-**32**	713	283	0.37	0.0518	0.0038	0.0078	0.0006	0.0011	0.00002	0.0003	0.00001	0.320	11	7.0	0.1	7.9	0.6	275	164	6.9	0.2	**7.0 ±**	**0.1**
TIB25-**15**	990	303	0.28	0.0514	0.0041	0.0079	0.0007	0.0011	0.00001	0.0004	0.00001	0.290	10	7.1	0.1	7.9	0.7	260	179	7.0	0.3	**7.1 ±**	**0.1**
TIB25-**7**	392	157	0.37	0.0607	0.0072	0.0097	0.0013	0.0012	0.00003	0.0004	0.00001	0.390	25	7.5	0.2	10	1.0	629	258	7.2	0.2	**7.5 ±**	**0.2**
TIB25-**38**	393	134	0.31	0.0555	0.0049	0.0096	0.0009	0.0013	0.00002	0.0004	0.00001	0.240	16	8.1	0.1	9.7	0.9	431	197	7.9	0.2	8.1 ±	0.1
TIB25-**10**	341	114	0.31	0.0502	0.0035	0.0091	0.0007	0.0013	0.00002	0.0004	0.00002	0.190	8	8.5	0.1	9.2	0.7	203	154	8.4	0.4	8.5 ±	0.1
TIB25-**35**	389	185	0.44	0.0546	0.0036	0.0149	0.0011	0.0020	0.00004	0.0006	0.00001	0.290	15	12.7	0.3	15	1.0	397	149	12.5	0.3	12.7 ±	0.3
TIB25-**34**	345	152	0.40	0.0645	0.0039	0.0181	0.0012	0.0020	0.00003	0.0006	0.00001	0.340	27	13.1	0.2	18	1.0	759	126	12.6	0.2	13.1 ±	0.2
TIB25-**37**	74	41	0.52	0.0613	0.0092	0.0172	0.0027	0.0021	0.00008	0.0008	0.00007	0.240	20	13.6	0.5	17	3.0	649	331	15.0	1.0	13.6 ±	0.5
TIB25-**3**	544	252	0.43	0.0605	0.0029	0.0213	0.0011	0.0026	0.00003	0.0008	0.00003	0.230	21	16.5	0.2	21	1.0	621	103	16.2	0.6	16.5 ±	0.2
TIB25-**13**	900	236	0.24	0.0491	0.0009	0.0713	0.0015	0.0105	0.00009	0.0036	0.00005	0.420	3	67.6	0.6	70	1.0	151	44	73.0	1.0	67.6 ±	0.6
TIB25-**16**	671	121	0.17	0.0496	0.0012	0.0928	0.0028	0.0136	0.00018	0.0043	0.00006	0.510	3	87.0	1.0	90	3.0	175	56	87.0	1.0	87.0 ±	1.0
TIB25-**20**	276	140	0.47	0.0540	0.0015	0.1053	0.0031	0.0142	0.00012	0.0045	0.00009	0.290	11	90.6	0.8	102	3.0	373	63	90.0	2.0	90.6 ±	0.8
TIB25-**31**	276	193	0.64	0.0517	0.0013	0.1014	0.0028	0.0142	0.00012	0.0044	0.00008	0.330	7	90.8	0.8	98	3.0	271	59	89.0	2.0	90.8 ±	0.8
TIB25-**21**	269	103	0.35	0.0504	0.0018	0.0989	0.0040	0.0142	0.00016	0.0045	0.00005	0.370	5	91.0	1.0	96	4.0	212	81	91.0	1.0	91.0 ±	1.0
TIB25-**39**	208	70	0.31	0.0464	0.0018	0.0907	0.0039	0.0142	0.00017	0.0045	0.00021	0.360	-3	91.0	1.0	88.0	4.0	19	80	91.0	4.0	91.0 ±	1.0
TIB25-**14**	215	100	0.43	0.0505	0.0016	0.0991	0.0033	0.0142	0.00013	0.0044	0.00011	0.270	5	91.1	0.8	96.0	3.0	220	74	89.0	2.0	91.1 ±	0.8
TIB25-**18**	264	171	0.60	0.0539	0.0029	0.1063	0.0060	0.0143	0.00014	0.0045	0.00005	0.200	11	91.6	0.9	103.0	6.0	366	120	90.2	0.9	91.6 ±	0.9
TIB25-**17**	264	139	0.49	0.0481	0.0013	0.0952	0.0026	0.0144	0.00013	0.0045	0.00009	0.340	0	92.0	0.8	92.0	2.0	104	60	91.0	2.0	92.0 ±	0.8
TIB25-**22**	300	138	0.42	0.0493	0.0011	0.0975	0.0023	0.0144	0.00012	0.0044	0.00009	0.370	2	92.0	0.8	94.0	2.0	163	51	89.0	2.0	92.0 ±	0.8
TIB25-**4**	181	64	0.33	0.0496	0.0024	0.0985	0.0054	0.0144	0.00021	0.0046	0.00008	0.450	3	92.0	1.0	95.0	5.0	178	110	92.0	2.0	92.0 ±	1.0
TIB25-**6**	180	67	0.34	0.0510	0.0022	0.1015	0.0045	0.0144	0.00014	0.0045	0.00014	0.230	6	92.3	0.9	98.0	4.0	241	98	91.0	3.0	92.3 ±	0.9
TIB25-**5**	452	177	0.36	0.0508	0.0017	0.1018	0.0037	0.0145	0.00020	0.0050	0.00012	0.400	5	93.0	1.0	98.0	3.0	229	76	100.0	2.0	93.0 ±	1.0
TIB25-**33**	241	72	0.28	0.0497	0.0018	0.1001	0.0039	0.0146	0.00015	0.0046	0.00005	0.310	4	93.5	1.0	97.0	4.0	182	81	93.0	1.0	93.5 ±	1.0
TIB25-**30**	710	215	0.28	0.0482	0.0010	0.1044	0.0023	0.0157	0.00014	0.0050	0.00008	0.420	0	100.7	0.9	101.0	2.0	111	47	101.0	2.0	100.7 ±	0.9
TIB25-**2**	237	87	0.34	0.0608	0.0022	0.1688	0.0089	0.0202	0.00050	0.0062	0.00015	0.630	18	129.0	3.0	158.0	8.0	631	79	125.0	3.0	129.0 ±	3.0
TIB25-**1**	1609	495	0.28	0.0871	0.0010	2.5152	0.0362	0.2096	0.00145	0.0621	0.00042	0.560	4	1227.0	8.0	1276.0	10.0	1362	21	1218.0	8.0	1362.0 ±	21.0
n = 31																						**Weighted $^{206}Pb/^{238}U$ mean age =**	**7.03 ± 0.19**
																						MSWD = 2.0; n = 5	

[#]U and Th concentrations (ppm) are calculated relative to analyses of trace-element glass standard NIST 612.

[†]Isotopic ratios ratios are corrected relative to PLE standard zircon for mass bias and down-hole fractionation (PLE, Plešovice = ~337 Ma; Sláma *et al*., 2008). Common Pb corrections were made using the Andersen Method (Andersen, 2002).

*All errors in isotopic ratios and ages are absolute and given at the 1-sigma level except for the Weighted Mean $^{206}Pb/^{238}U$ age that is reported at the 2-sigma level.

**Percentage discordance obtained using the following equation (100*[(age $^{207}Pb/^{235}U$)-(age $^{206}Pb/^{238}U$)]/age $^{207}Pb/^{235}U$). Positive and negative values indicate normal and inverse discordance, respectively.

Individual zircon ages in bold were used to calculate the weighted mean $^{206}Pb/^{238}U$ age and MSWD (Mean Square of Weigthed Deviates) using the computacional program Isoplot (Ludwig , 2003).

Figure 1

Bennett et al_FIGURES

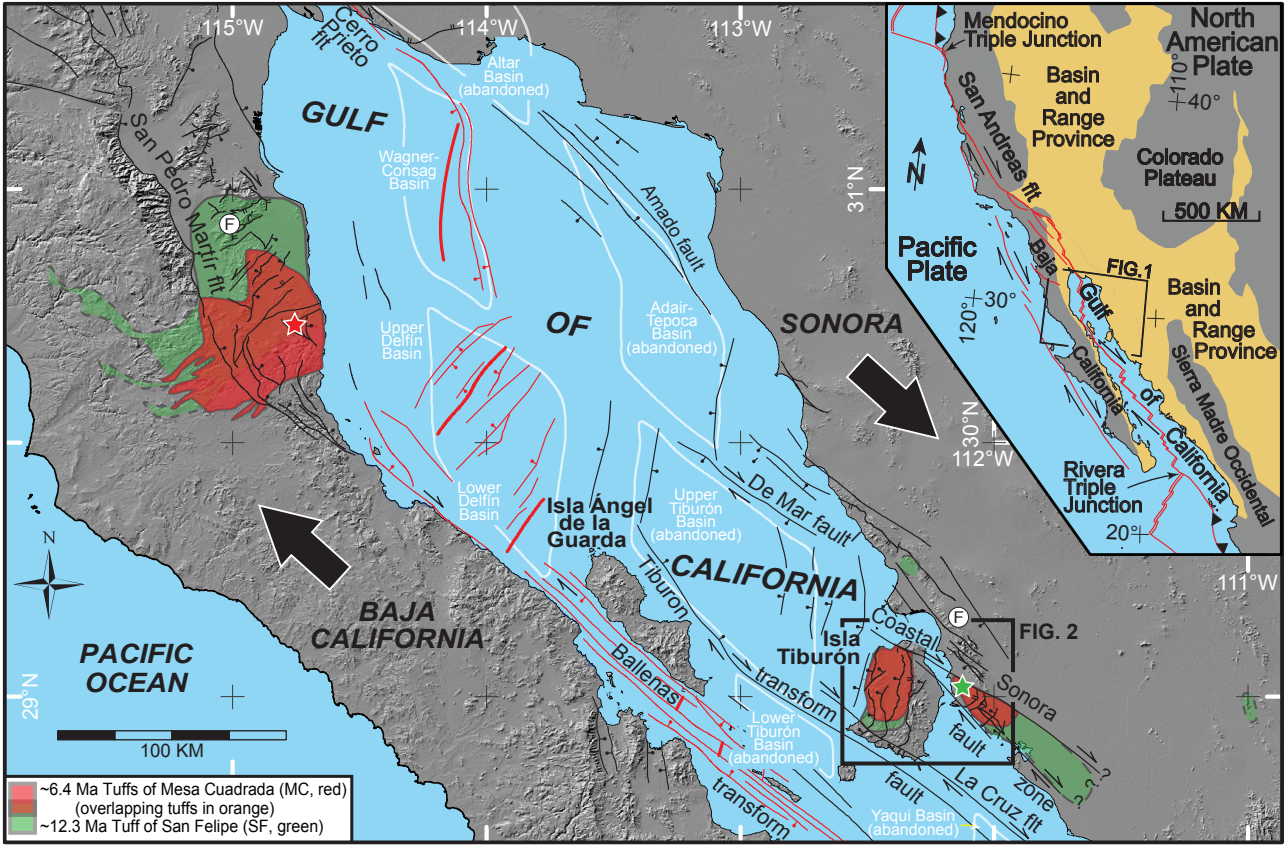

Figure 2

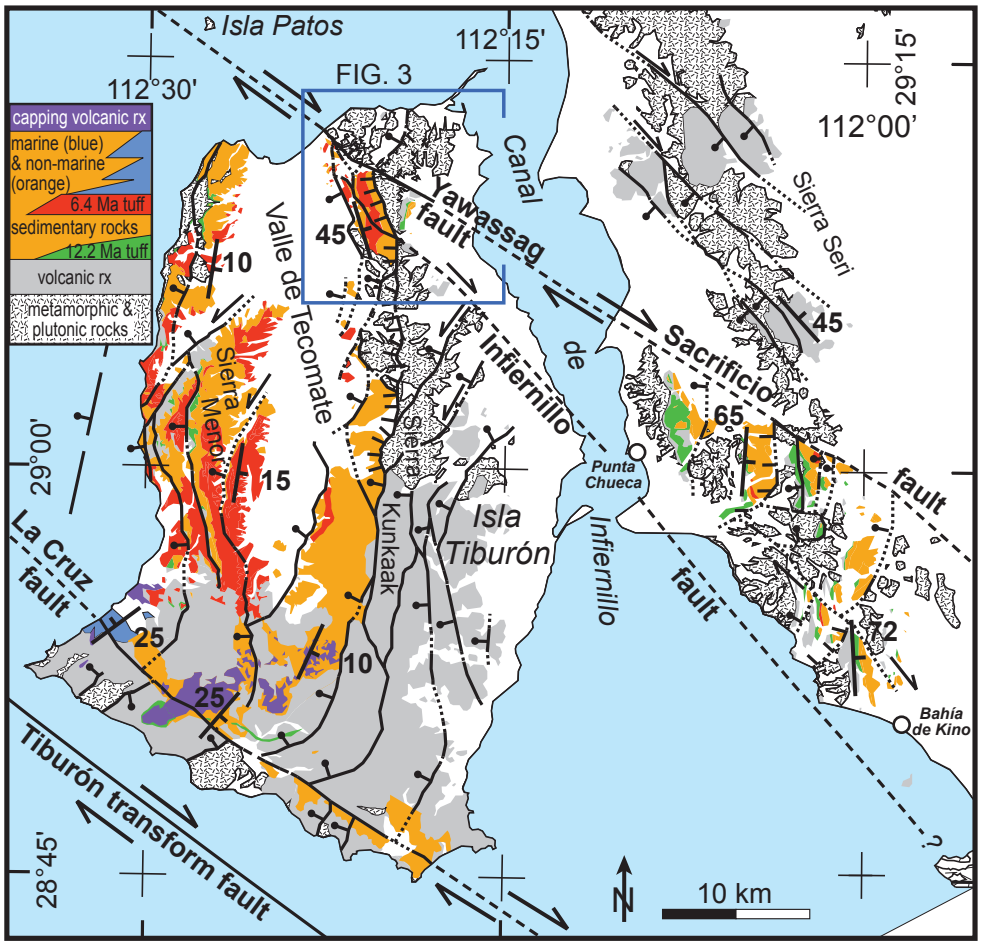
Isla Patos
112°30'
112°15'
FIG. 3
29°15'
112°00'
capping volcanic rx
marine (blue) & non-marine (orange)
6.4 Ma tuff
sedimentary rocks
12.2 Ma tuff
volcanic rx
metamorphic & plutonic rocks
Canal
Yawassag fault
Valle de Tecomate
Sierra Seri
Sierra Menor
Sierra Kunkaak
Infiernillo
Sacrificio
Punta Chueca
Isla Tiburón
Infiernillo fault
fault
La Cruz fault
Tiburón transform fault
Bahía de Kino
29°00'
28°45'
45
10
15
25
65
12
N
10 km

FIGURE 3
Geologic map of northeast Isla Tiburón
Mapping conducted 2009 - 2010
by Scott E.K. Bennett

0 1 2 KM
1:15,000

N

GULF OF CALIFORNIA (SEA OF CORTEZ)

CANAL

Ancuacoop (Punta Perla)

Zozni

DE

Coniic

Hinoc Himaitom

INFIERNILLO

Canoa Canipai (Playa Tecomate)

Yawassag

Cotéhan

SIERRA

KUNKAAK

Tecomate

Hast Xepenocap

Hast Hinzime

Hinzime

Sepoc Hancaap

Kunkaak

Yawassag fault

fault

Inﬁernillo fault

Valle de las Aguilas

Valle de Tecomate

LIMIT OF MAPPING

LIMIT OF MAPPING

A — A'

B — B'

C — C'

83.4 ± 0.9 U/Pb (zircon)

84.4 ± 0.9 U/Pb (zircon)

reworked ash bed

Tecomate Ash Bed
7.11 ± 0.09 Ar/Ar (k-spar)
7.03 ± 0.19 U/Pb (zircon)

90.4 ± 2.7
K-Ar (hornblende)

77.7 ± 3.1
Rb-Sr (biotite-WR)

81.4 ± 3.2
Rb-Sr (biotite-WR)

Datum: WGS84
Projection:UTM Zone12N
10 m Contour Interval

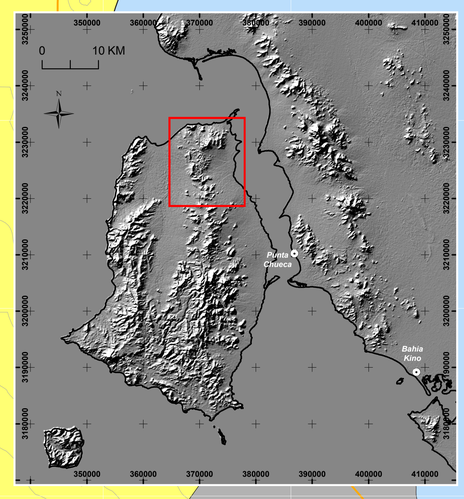

Map Units

Era	Period	Epoch		
Cenozoic	Quaternary	Pleist. - Holocene	Qae	Aeolian deposits
			Qal	Alluvial sand and gravel
			Qb	Beach sand to cobbles
			Qoa	Old non-marine terrace deposits
			Qm	Marine terrace deposits
	Neogene	Miocene	Tcg3	Non-marine conglomerate
			Tmr4	Tuffs of Mesa Cuadrada (~6.4 Ma)
			T3t	
			Tmr3	
			Trsh3	Rhyolite Flows of Sepoc Hancaap, unit 3
			Tcg3	Non-marine conglomerate
			Tsg	Greenish-yellow volcani-clastic sandstone
			Tb2	Basalt flow, unit 2
			Trsh2	Rhyolite Flows of Sepoc Hancaap, unit 2
			Tcg1	Non-marine conglomerate
			Tbv	Vesicular basalt
			Ttsf	Tuff of San Felipe (~12.2 Ma)
			Trsh1	Rhyolite Flows of Sepoc Hancaap, unit 1
			Tb1	Basalt flow, unit 1
			Tha	Hornblende-rich andesite
			Tba	Basaltic-andesite
			Tcb	Basal non-marine conglomerate
			Tbhh	Silicified tuff breccia
			Trhh	Rhyolite of Hast Hinzime
Mesozoic	Cretaceous	L. Cretaceous	Kgd	Granodiorite
			Kd	Diorite
			Kt	Tonalite
Paleozoic	?	?	Pz	Metasedimentary rocks

Geochronologic Sample (Age (Ma) and technique)

paleomagnetic drill site of Bennett and Oskin (2014)

unimproved dirt road graded in 1960's

Contacts

contact - certain, approx., queried, concealed (dip shown where measured)

fault - certain, approx., queried, concealed (dip and rake shown where measured)

Structures (dip shown)

bedding - inclined, approx., overturned, horizontal

eutaxitic foliation - inclined, vertical joint - inclined

fault - inclined, vertical, with striae (rake shown)

contact - inclined, horizontal

anticline axis

syncline axis

normal fault, thrust fault, strike-slip fault

felsic dike

FIGURE 5

Tecomate ash bed (interbedded in 'Tcg3' of the Tecomate Basin)

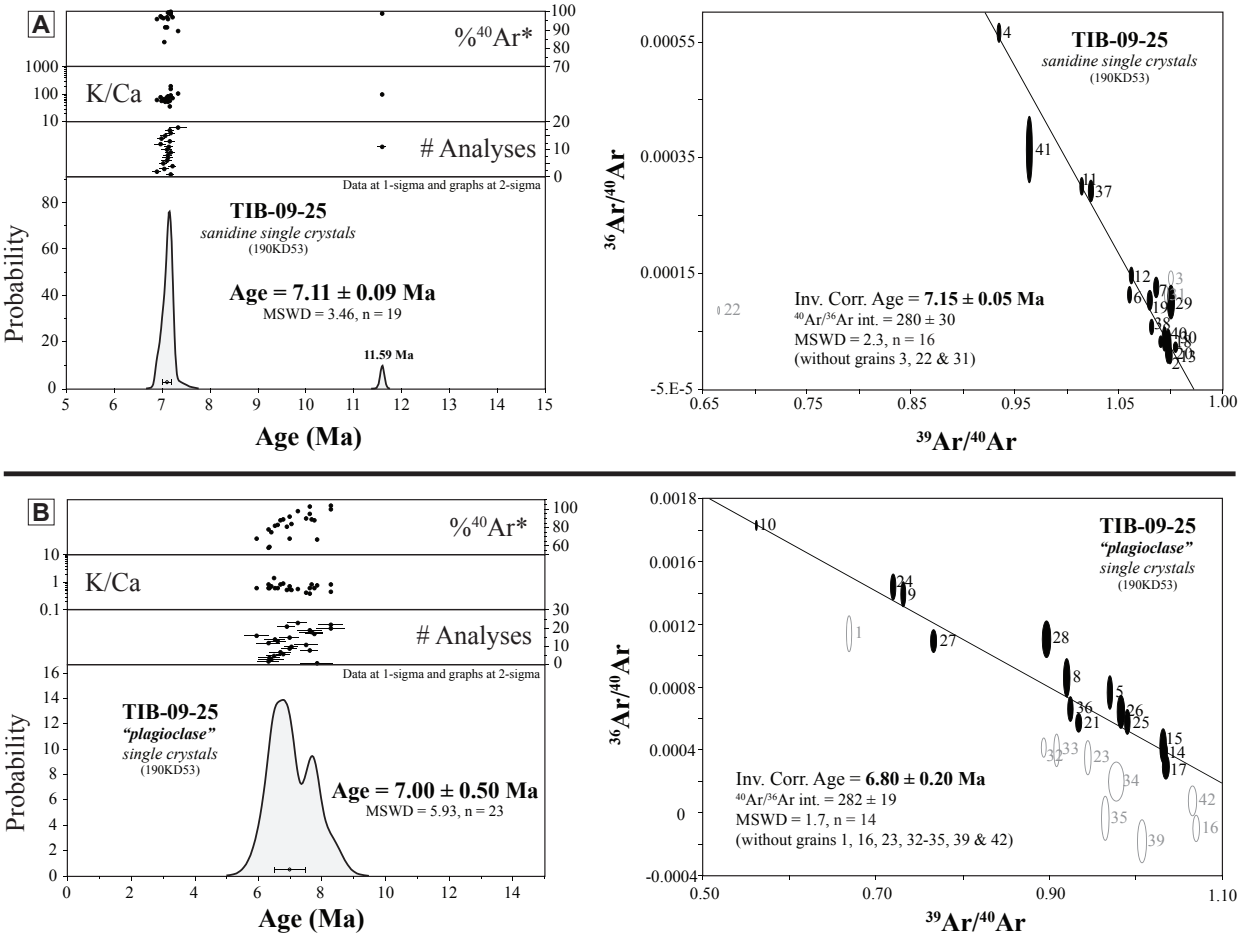

FIGURE 6

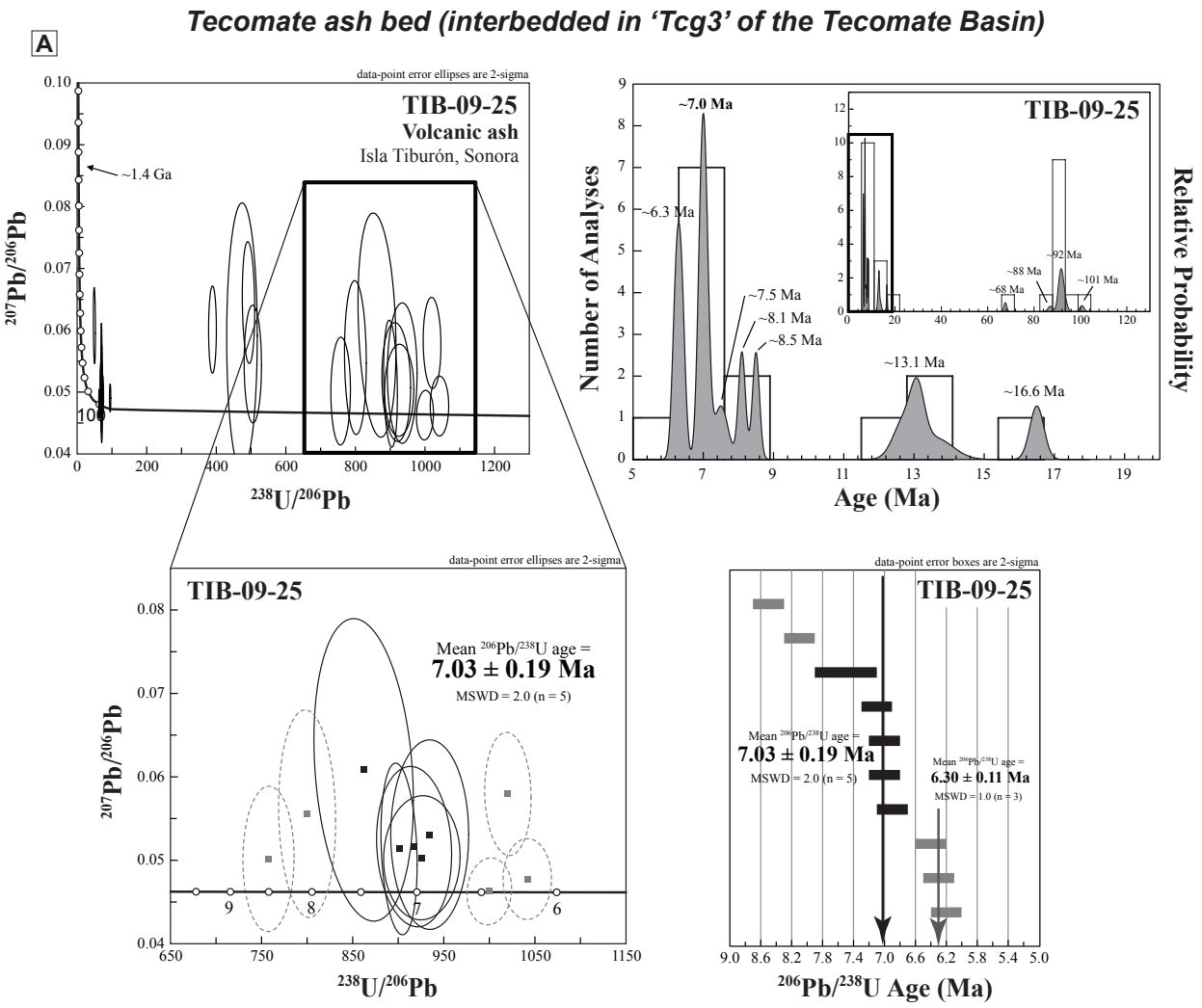
Tecomate ash bed (interbedded in 'Tcg3' of the Tecomate Basin)
A
data-point error ellipses are 2-sigma
TIB-09-25
Volcanic ash
Isla Tiburón, Sonora
~1.4 Ga
100
^{207}Pb/^{206}Pb
^{238}U/^{206}Pb
TIB-09-25
~7.0 Ma
~6.3 Ma
~7.5 Ma
~8.1 Ma
~8.5 Ma
~13.1 Ma
~16.6 Ma
~92 Ma
~88 Ma
~68 Ma
~101 Ma
Number of Analyses
Relative Probability
Age (Ma)
data-point error ellipses are 2-sigma
TIB-09-25
Mean ^{206}Pb/^{238}U age =
7.03 ± 0.19 Ma
MSWD = 2.0 (n = 5)
^{207}Pb/^{206}Pb
^{238}U/^{206}Pb
data-point error boxes are 2-sigma
TIB-09-25
Mean ^{206}Pb/^{238}U age =
7.03 ± 0.19 Ma
MSWD = 2.0 (n = 5)
Mean ^{206}Pb/^{238}U age =
6.30 ± 0.11 Ma
MSWD = 1.0 (n = 3)
^{206}Pb/^{238}U Age (Ma)

FIGURE 7A

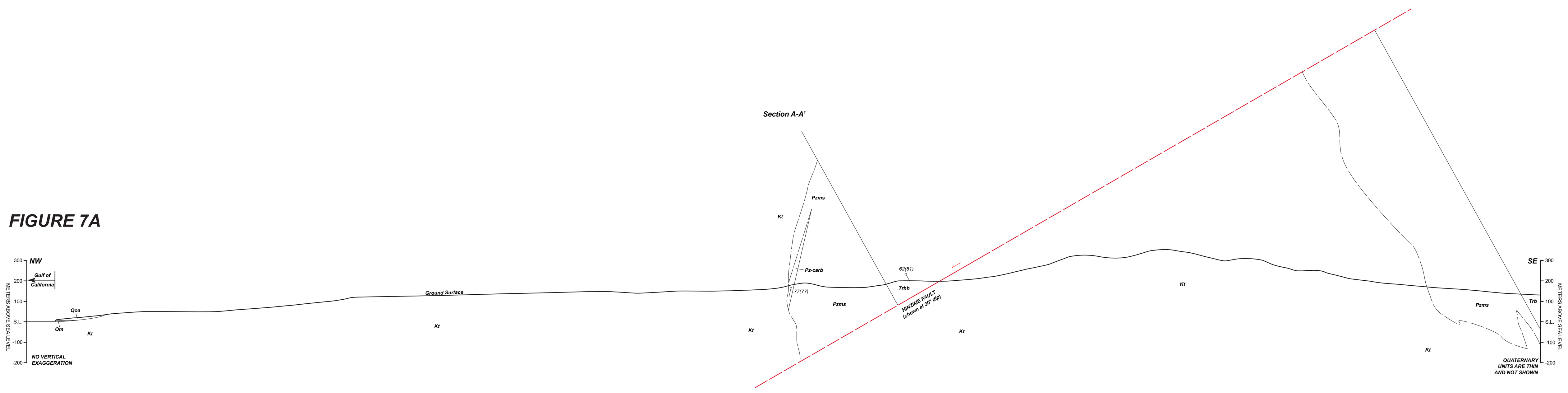

Section A-A'
NW
SE
Gulf of California
METERS ABOVE SEA LEVEL
300
200
100
S.L.
-100
-200
Qoa
Qm
Kt
Ground Surface
Pzms
Pz-carb
77(77)
62(61)
Trhh
HINZIME FAULT (shown at 30° dip)
Trb
NO VERTICAL EXAGGERATION
QUATERNARY UNITS ARE THIN AND NOT SHOWN

FIGURE 7B

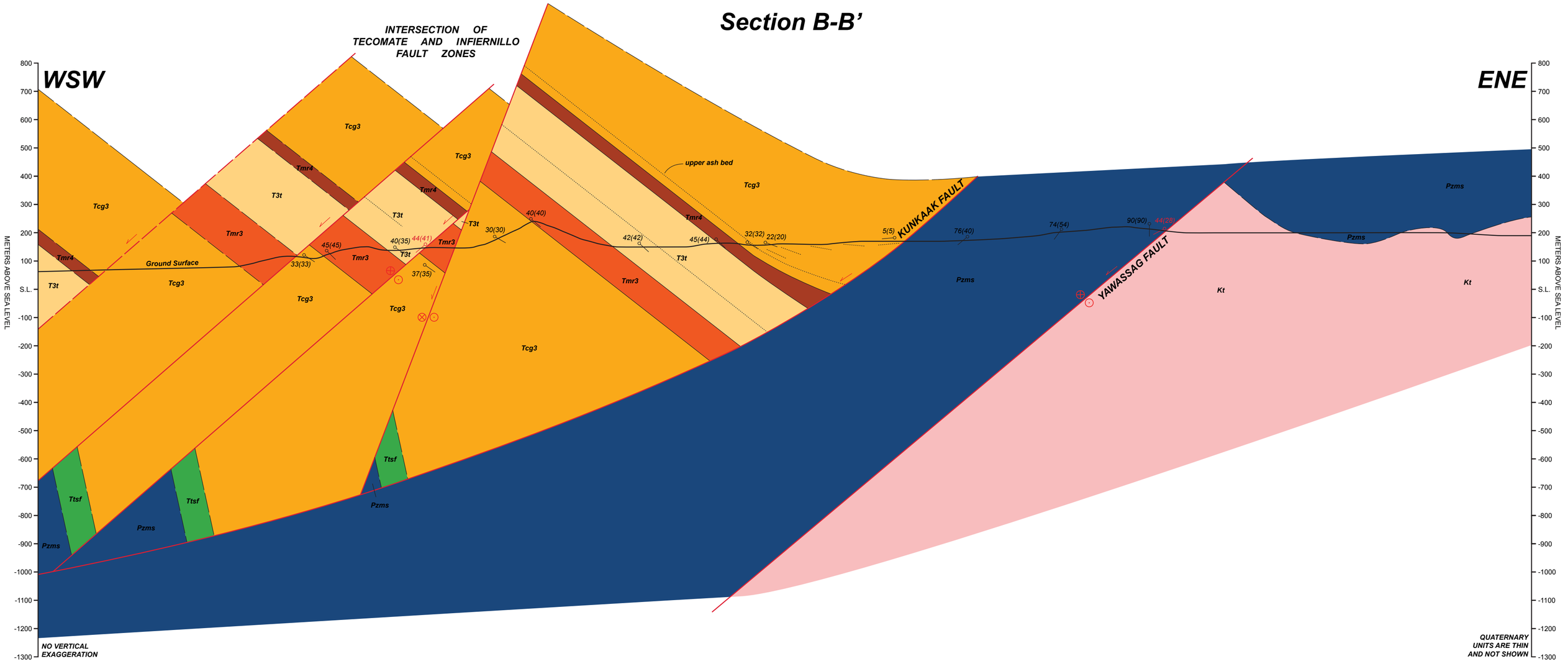
Section B-B'
INTERSECTION OF TECOMATE AND INFIERNILLO FAULT ZONES
WSW
ENE
METERS ABOVE SEA LEVEL
S.L.
800
700
600
500
400
300
200
100
-100
-200
-300
-400
-500
-600
-700
-800
-900
-1000
-1100
-1200
-1300
Tcg3
Tmr4
T3t
Tmr3
Ttsf
Pzms
Kt
upper ash bed
Ground Surface
KUNKAAK FAULT
YAWASSAG FAULT
45(45)
40(35)
44(41)
33(33)
37(35)
30(30)
40(40)
42(42)
45(44)
32(32)
22(20)
5(5)
76(40)
74(54)
90(90)
44(28)
NO VERTICAL EXAGGERATION
QUATERNARY UNITS ARE THIN AND NOT SHOWN

FIGURE 7C

Section C-C'